Available online at www.sciencedirect.com
SCIENCE DIRECT®
C. R. Mecanique 333 (2005) 397–404
COMPTES RENDUS MECANIQUE
http://france.elsevier.com/direct/CRAS2B/

An adaptation of the low Mach number approximation for supercritical fluid buoyant flows

Gilbert Accary [a,*], Isabelle Raspo [a], Patrick Bontoux [a], Bernard Zappoli [b]

[a] *Laboratoire de modélisation et simulation numérique en mécanique, UMR 6181 du CNRS, les universités Aix-Marseille, technopôle de Château Gombert, 38, rue Frédéric-Joliot-Curie, 13451 Marseille cedex 20, France*
[b] *CNES, 18, avenue Edouard-Belin, 31401 Toulouse cedex 4, France*

Received 7 June 2004; accepted 8 March 2005

Presented by René Moreau

Abstract

This Note describes an acoustic filtering of the equations governing the supercritical fluid buoyant flow driven by a weak heating. The resulting low Mach number approximation takes into account the compressibility of the fluid with respect to the hydrostatic pressure. Using the direct numerical simulation of a supercritical fluid flow in the Rayleigh–Bénard configuration, we show that the density stratification may be taken into account without further numerical effort and is fundamental for the prediction of the convective instability threshold induced by a weak heating. ***To cite this article: G. Accary et al., C. R. Mecanique 333 (2005).***

Résumé

Une adaptation de l'approximation faible nombre de Mach aux écoulements de convection naturelle dans les fluides supercritiques. Cette Note décrit un filtrage acoustique des équations régissant la convection naturelle dans un fluide supercritique due à un faible chauffage. L'approximation faible nombre de Mach obtenue prend en compte la compressibilité du fluide par rapport à la pression hydrostatique. Par la simulation numérique directe de l'écoulement d'un fluide supercritique en configuration de Rayleigh–Bénard, nous montrons que la stratification en densité peut être prise en compte sans effort numérique supplémentaire et qu'elle est fondamentale pour la prédiction du seuil d'instabilité convective induite par un faible chauffage. ***Pour citer cet article : G. Accary et al., C. R. Mecanique 333 (2005).***

Keywords: Fluid mechanics; Supercritical fluid; Low Mach number; Rayleigh–Bénard instability; Piston effect

* Corresponding author.
E-mail address: accary@L3m.univ-mrs.fr (G. Accary).

1631-0721/$ – see front matter
doi:10.1016/j.crme.2005.03.004

Mots-clés : Mécanique des fluides ; Fluide supercritique ; Faible nombre de Mach ; Instabilité de Rayleigh–Bénard ; Effet piston

Version française abrégée

Dans les simulations numériques directes (DNS) d'écoulements de fluides supercritiques (FSC) en configuration de Rayleigh–Bénard [1–3], le modèle mathématique [13] est résolu dans une approximation à faible nombre de Mach (FNM) qui fait intervenir la stratification en densité alors que le filtrage acoustique classique des équations proposé dans [14] suggère un champ de densité initial homogène. La validité de cette modélisation est discutée ici pour la prédiction de l'instabilité convective.

Une couche de FSC d'épaisseur L est contenue entre deux plaques horizontales infinies (Fig. 1). Le fluide est initialement en équilibre thermodynamique à température constante T_i légèrement supérieure à la température critique T_c, et stratifié en densité et en pression. La simulation numérique commence par l'application d'un faible chauffage à la plaque inférieure ($\Delta T \sim$ quelques mK) tout en maintenant la plaque supérieure à sa température initiale. Le modèle mathématique proposé dans [13] est considéré pour le CO_2 avec $T_i - T_c = 1$ K.

Soit V, T_c, ρ_c et $R\rho_c T_c$ les échelles respectives de la vitesse $\boldsymbol{v}$, de la température T, de la densité ρ et de la pression P, où V est une vitesse caractéristique de l'écoulement, ρ_c est la densité critique et R est la constante des gaz parfaits. Les variables d'espace $\boldsymbol{x}(x, y)$ et de temps t sont respectivement adimensionnées par L et L/V. Pour un faible nombre de Mach (Ma), les variables primaires sont développées en séries de Ma^2 [14]. Les ordres O(1) et O(Ma^2) du bilan de quantité de mouvement sont respectivement donnés par les Éqs. (2) et (3), où l'exposant 0 (resp. 1) désigne les termes d'ordre 1 (resp. Ma^2), $\gamma = 1.4$ est l'exposant adiabatique du gaz parfait, $\boldsymbol{e}_g$ est le vecteur unitaire parallèle à la gravité terrestre $\boldsymbol{g}$, Fr et Re sont respectivement les nombres de Froude et de Reynolds. Dans ces équations, on suppose que $\mathrm{O}(Ma^2/Fr) > \mathrm{O}(Ma^2)$ puisque, du fait de la divergence de la compressibilité du FSC, la pression hydrostatique entraîne une variation de densité du même ordre que celle induite par le faible chauffage considéré (quelques mK). En négligeant la variation de la masse volumique $\delta\rho^{(0)}$ devant le champ de densité initial stratifié $\rho_i = \rho_s$, les ordres O(1) et O(Ma^2) du bilan de quantité de mouvement sont finalement décrits par les Éqs. (4) et (5) respectivement, avec $\Pi = P^{(0)} - P_s$ où P_s est la pression hydrostatique. Le filtrage acoustique des autres équations (continuité, énergie et équation d'état de van der Waals) est réalisé comme dans [14] ; le modèle obtenu noté FNMA (pour FNM Adapté aux FSC) diffère légèrement (par $\rho_i \neq 1$) du modèle FNMC (pour FNM Classique) dans lequel la compressibilité du FSC est complètement négligée. Ces deux modèles sont résolus pour les mêmes paramètres numériques par une méthode du type volumes finis [15], le domaine de calcul étant un carré de côté L avec des conditions périodiques dans la direction x.

Pour différents cas de chauffage, la Fig. 2 montre l'évolution de la perturbation de température δT dans la couche limite chaude d'épaisseur h induite par le chauffage de la plaque inférieure. La zone d'instabilité est délimitée par la ligne pleine et épaisse déduite du critère établi dans [5,6] comportant l'effet stabilisateur du gradient adiabatique de température (critère de Schwarzchild) lié à la pression hydrostatique. Les symboles correspondent aux instants d'effondrement de la couche limite chaude provoqué par l'apparition des panaches thermiques générés par l'instabilité convective. Pour les faibles chauffages, les variations de densité d'origine thermique deviennent du même ordre que celles dues à la stratification ; le modèle FNMA reproduit bien l'allure de la courbe de stabilité et aucune déformation couche limite chaude n'est observée pour $\Delta T < 0{,}2$ mK ; par contre le modèle FNMC, ne tenant pas compte de l'effet stabilisateur de la pression hydrostatique, continue à prédire une instabilité convective selon le critère de Rayleigh classique obtenu en ignorant le gradient adiabatique de température. Pour $\Delta T = 0{,}3$ mK, la Fig. 3 montre les champs instantanés de température $100t_{\mathrm{EP}}$ secondes après l'effondrement de la couche limite chaude (t_{EP} est l'échelle de temps caractéristique de l'effet piston responsable de l'équilibre rapide de la température dans les FSC [9–12]) ; les panaches thermiques obtenus avec le modèle FNMC sont nettement plus développés que ceux prédits par le modèle FNMA et se déplacent plus vite puisque leur mouvement n'est pas gêné par la stratification.

1. Introduction

Direct numerical simulations (DNS) of supercritical fluid (SCF) flows in the Rayleigh–Bénard configuration [1–4] contribute, together with theoretical studies [5,6] and experimental investigations [7,8], to a better understanding of the interaction between natural convection and the 'piston effect' (PE). This thermoacoustic is known to control the fast temperature equilibrium in a fluid close to its gas–liquid critical point [9–12].

In the numerical approach [1–3], the mathematical model of a SCF flow, proposed in [13], is solved in a low Mach number (LMN) approximation which involves the density stratification while the classical acoustic filtering of the governing equations [14] suggests a homogeneous initial density field for a reasonable size container. Indeed, for the weak heating considered in these works (a few mK) and owing to the divergence of the isothermal compressibility of the SCF, the density perturbations caused by the hydrostatic pressure become of the same order as those induced by heating as this latter gets weaker.

The aim of this article is to discuss the validity and the limits of this LMN approximation taking into account the compressibility of the SCF with respect to the hydrostatic pressure. The resulting model is compared to its counterpart (not including the density stratification) for the prediction of a SCF flow in the Rayleigh–Bénard configuration. The comparisons concern the convection threshold criterion established in [5,6] as well as the temperature patterns.

2. The problem under investigation

For the sake of clarity and conciseness, the acoustic filtering is performed straightaway on the equations governing the SCF flow in the Rayleigh–Bénard configuration shown in Fig. 1. A fluid layer of thickness L ($L = 1$ cm) is enclosed between two plates and subjected to the earth gravitational field $\boldsymbol{g}$, the plates are supposed infinite. No slip conditions are imposed on these boundaries. Initially, the fluid is in thermodynamic equilibrium at a constant temperature T_i slightly above the critical temperature T_c such that $T_i = (1+\varepsilon)T_c$, where ε defines the dimensionless proximity to the critical point ($\varepsilon \ll 1$). Under the effect of its weight, the fluid is stratified with a mean density equal to its critical value ρ_c. The simulation starts with the application of a weak heating ($\Delta T \sim$ few mK) at the bottom plate while maintaining the top one at its initial temperature T_i.

The mathematical model for a SCF flow [13] is described by the Navier–Stokes and energy equations written for a Newtonian and highly conducting van der Waals fluid. The van der Waals equation of state yields to a critical divergence as ε^{-1} of the thermal expansion coefficient, of the isothermal compressibility, and of the heat capacity at constant pressure. A $(1 + \Lambda(T/T_c - 1)^{-1/2})$ law, with $\Lambda = 0.75$ is used to describe the critical divergence of the thermal conductivity, while the heat capacity at constant volume and the dynamic viscosity are those of a perfect gas. In this study, we consider carbon dioxide near its critical conditions ($T_c = 304.13$ K, $\rho_c = 467.8$ Kg m^{-3}, $P_c = 7.38$ MPa) and the corresponding transport properties.

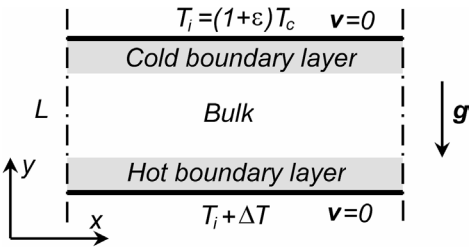

Fig. 1. A supercritical fluid in the Rayleigh–Bénard configuration.

Fig. 1. Un fluide supercritique en configuration de Rayleigh–Bénard.

3. Acoustic filtering

In the following, we only detail the acoustic filtering of the momentum equation since the LMN approximation of the other governing equations (continuity, energy, and state) is identical to the commonly used one, set up for a perfect gas [14].

In order to make the variables dimensionless, let V, T_c, ρ_c, and $R\rho_c T_c$ be respectively representative scales of the velocity $\boldsymbol{v}$, the temperature T, the density ρ, and the pressure P; where R is the perfect gas constant and V is a characteristic speed of the flow (defined later). On the other hand, the independent spatial variables $\boldsymbol{x}(x, y)$ and time t are referenced respectively by L and L/V. The resulting dimensionless momentum equation is written as follows:

$$\frac{\partial(\rho \boldsymbol{v})}{\partial t} + \nabla \cdot (\rho \boldsymbol{v}\boldsymbol{v}) = -\frac{1}{\gamma\, Ma^2}\nabla P + \frac{1}{Re}\left[\nabla^2 \boldsymbol{v} + \frac{1}{3}\nabla(\nabla \cdot \boldsymbol{v})\right] + \frac{\boldsymbol{e}_g}{Fr}\rho \tag{1}$$

where $\gamma = 1.4$ is the isentropic exponent of a perfect gas, and $\boldsymbol{e}_g$ is the unit vector in the direction of $\boldsymbol{g}$. Ma, Re, and Fr are respectively the Mach, Reynolds, and Froude numbers defined as:

$$Ma = \frac{V}{c_0}, \quad Re = \frac{\rho_c V L}{\mu}, \quad Fr = \frac{V^2}{gL}$$

where $c_0 = \sqrt{\gamma R T_c}$ is the sound speed and μ is the dynamic viscosity.

Assuming that $Ma \ll 1$, all the primary variables of the problem gathered by the vector $\boldsymbol{\Phi} =^t (\boldsymbol{v}, T, P, \rho)$ can be expanded in series of Ma^2 as follows:

$$\boldsymbol{\Phi} = \boldsymbol{\Phi}^{(0)} + \gamma\, Ma^2 \boldsymbol{\Phi}^{(1)} + \mathrm{o}(Ma^2) \quad \text{where } \boldsymbol{\Phi}^{(0)} \text{ and } \boldsymbol{\Phi}^{(1)} \text{ are O(1)}$$

The O(1) and O(Ma^2) parts of the momentum equation (1) resulting from this expansion are given by:

$$\mathrm{O}(1)\colon\ 0 = -\nabla P^{(0)} + \frac{\gamma\, Ma^2}{Fr}\rho^{(0)}\boldsymbol{e}_g \tag{2}$$

$$\mathrm{O}(Ma^2)\colon\ \frac{\partial(\rho^{(0)}\boldsymbol{v}^{(0)})}{\partial t} + \nabla \cdot \left(\rho^{(0)}\boldsymbol{v}^{(0)}\boldsymbol{v}^{(0)}\right) = -\nabla P^{(1)} + \frac{\gamma\, Ma^2}{Fr}\rho^{(1)}\boldsymbol{e}_g + \frac{1}{Re}\left[\nabla^2 \boldsymbol{v}^{(0)} + \frac{1}{3}\nabla\left(\nabla \cdot \boldsymbol{v}^{(0)}\right)\right] \tag{3}$$

In writing Eqs. (2) and (3), we supposed that $Ma^2/Fr > \mathrm{O}(Ma^2)$. This hypothesis is the heart of the matter since, as it will be shown next, keeping the buoyancy term $(\gamma\, Ma^2/Fr)\rho^{(0)}\boldsymbol{e}_g$ in the leading order of the momentum equation directly implies the introduction of the density and pressure stratifications in the final model. In addition, $Ma^2/Fr = gL/c_0^2$ is not related to Ma, therefore the inclusion of the buoyancy term at O(1) or at O(Ma^2) does not rely on the LMN assumption but is associated to the magnitude of this term in comparison to other leading mechanisms in the flow. As mentioned in the introduction, owing to the divergence of the isothermal compressibility of the SCF, the hydrostatic pressure induces a density variation comparable to that resulting from a weak heating.

The choice of retaining the buoyancy force at O(1) may seem inducing additional computational effort at first sight since for solving Eq. (3) one must now provide $\rho^{(1)}$ which requires, as pointed out by Paolucci [14], the resolution of all the O(Ma^2) governing equations. In order to keep a simple model, we make use of the fact that heating is weak. In this case, $\rho^{(0)}$ can be written as:

$$\rho^{(0)} = \rho_s + \delta\rho^{(0)}$$

where ρ_s is the initial density field that includes the density stratification $\delta\rho_s$, $\rho_s = 1 + \delta\rho_s$ is O(1). The maximum value of $\delta\rho^{(0)}$ takes place at the heated bottom plate; in the case of CO_2 with $T_i - T_c = 1$ K and for a heating $\Delta T = 1$ mK, $\delta\rho^{(0)} < 0.66 \times 10^{-3}$. The approximation consists of dropping $\delta\rho^{(0)}$ in comparison with ρ_s in Eq. (2) to obtain:

$$\mathrm{O}(1)\colon\ 0 = -\nabla P^{(0)} + \frac{\gamma\, Ma^2}{Fr}\rho_s \boldsymbol{e}_g$$

In the initial static equilibrium, the hydrostatic pressure P_s is such that: $\nabla P_s = (\gamma\, Ma^2/Fr)\rho_s \boldsymbol{e}_g$.

It is convenient to define a pressure $\Pi = P^{(0)} - P_s$ and the O(1) momentum equation is then given by:

$$\mathrm{O}(1)\text{: } \nabla \Pi = 0 \tag{4}$$

Thus Π is only a function of time and the thermodynamic pressure $P^{(0)}$ is deduced from $P^{(0)} = \Pi + P_s$. The term $(\gamma\, Ma^2/Fr)\delta\rho^{(0)}\boldsymbol{e}_g$ put aside in Eq. (2) must be inevitably included as $(1/Fr)\delta\rho^{(0)}\boldsymbol{e}_g$ in the O(Ma^2) momentum equation which can be written as follows:

$$\mathrm{O}(Ma^2)\text{: } \frac{\partial(\rho^{(0)}\boldsymbol{v}^{(0)})}{\partial t} + \nabla\cdot\left(\rho^{(0)}\boldsymbol{v}^{(0)}\boldsymbol{v}^{(0)}\right) = -\nabla P^{(1)} + \left(\delta\rho^{(0)} + \gamma\, Ma^2\rho^{(1)}\right)\frac{\boldsymbol{e}_g}{Fr} + \frac{1}{Re}\left[\nabla^2\boldsymbol{v}^{(0)} + \frac{1}{3}\nabla\left(\nabla\cdot\boldsymbol{v}^{(0)}\right)\right]$$

With no additional assumption to the LMN one, the term $(\gamma\, Ma^2/Fr)\rho^{(1)}\boldsymbol{e}_g$ compared to $(1/Fr)\delta\rho^{(0)}\boldsymbol{e}_g$ may be neglected in the previous equation and should instead appear at O(Ma^4) as $(1/Fr)\rho^{(1)}\boldsymbol{e}_g$. The O($Ma^2$) of the momentum equation is finally given by:

$$\mathrm{O}(Ma^2)\text{: } \frac{\partial(\rho^{(0)}\boldsymbol{v}^{(0)})}{\partial t} + \nabla\cdot\left(\rho^{(0)}\boldsymbol{v}^{(0)}\boldsymbol{v}^{(0)}\right) = -\nabla P^{(1)} + \frac{1}{Fr}\left(\rho^{(0)} - \rho_s\right)\boldsymbol{e}_g + \frac{1}{Re}\left[\nabla^2\boldsymbol{v}^{(0)} + \frac{1}{3}\nabla\left(\nabla\cdot\boldsymbol{v}^{(0)}\right)\right] \tag{5}$$

Eqs. (4) and (5) must be completed with the time-independent expressions of P_s and ρ_s obtained by solving the static equilibrium coupled to the van der Waals equation of state with the additional condition that the mean value of ρ_s is equal to 1. The acoustic filtering of the other governing equations (continuity, energy, and state) is done as in [14], and the LMN model adapted for a SCF flow driven by a weak heating is given below after dropping the zero superscripts.

$$\frac{\partial\rho}{\partial t} + \nabla\cdot(\rho\boldsymbol{v}) = 0$$

$$\frac{\partial(\rho\boldsymbol{v})}{\partial t} + \nabla\cdot(\rho\boldsymbol{v}\boldsymbol{v}) = -\nabla P^{(1)} + \frac{1}{\psi}\left[\nabla^2\boldsymbol{v} + \frac{1}{3}\nabla(\nabla\cdot\boldsymbol{v})\right] + \frac{\boldsymbol{e}_g}{Fr}(\rho - \rho_s)$$

$$\frac{\partial(\rho T)}{\partial t} + \nabla\cdot(\rho\boldsymbol{v}T) = -(\gamma-1)(\Pi + P_s + a\rho^2)(\nabla\cdot\boldsymbol{v}) + \frac{\gamma}{\psi\, Pr}\nabla\cdot\left[\left(1 + \Lambda(T-1)^{-1/2}\right)\nabla T\right]$$

$$\Pi + P_s = \frac{\rho T}{1-b\rho} - a\rho^2$$

$$\nabla\Pi = 0$$

$$\rho_s = \frac{k_1}{\mathrm{e}^{k_1} - 1}\mathrm{e}^{k_1 y} \quad \text{and} \quad P_s = k(\rho_s - 1) \quad \text{where } k = \frac{1+\varepsilon}{(1-b)^2} - 2a \text{ and } k_1 = -\frac{1}{k}\frac{\gamma\, Ma^2}{Fr}$$

This model features the 'Piston Effect' time scale $t_{\mathrm{PE}} = \psi^{-1}(\rho_c L^2)/\mu$ [13], with $\psi = \varepsilon^{-1}(1/\Lambda + \varepsilon^{-1/2})$, which is ψ times shorter than the molecular diffusion one; for CO_2 with $T_i - T_c = 1$ K, $\psi = 5709.5$. In this case, the characteristic velocity of the flow is $V = \psi\mu/(\rho_c L)$. Pr is the Prandtl number for a perfect gas, $b = 1/3$ and $a = 9/8$ are the dimensionless parameters of the van der Waals equation of state.

The initial conditions for this model are: $\boldsymbol{v} = 0$, $P^{(1)} = 0$, $T = 1 + \varepsilon$, $\rho = \rho_s$, and $\Pi = \frac{1+\varepsilon}{1-b} - a$.

It is worth underling that the pressure Π, as the thermodynamic pressure $P^{(0)}$ in the classical LMN approximation, is homogeneous in space and is computed using the mass conservation. By assigning $\rho_s = 1$, we exactly recover the classical LMN approximation in which the buoyancy term is dropped from the O(1) momentum equation; in that case $P_s = 0$ and Π becomes $P^{(0)}$.

4. Numerical method

The governing equations are solved using a fully implicit finite volume method on a staggered mesh. The method is second order accurate in space and third order in time and has been thoroughly validated on an analytical solution and on several benchmark natural convection test problems [15]. The computational domain is a square of side L. Periodic conditions are imposed in the x-direction. The dimensions of the grid used in the numerical calculations depend on the heating applied to the bottom plate, the finest being of (140×160) grid points. To obtain a better representation of the flow in the boundary layers, the mesh is refined with a power 2 law near the bottom and top walls while it is uniform in the horizontal direction.

5. Results

Simulations were carried out for $T_i - T_c = 1$ K. The model described above, denoted ALMN (for Adapted LMN), is compared, for the same simulation conditions, to the CLMN model (for Classical LMN) not including the density stratification and obtained from the first formulation by simply setting $\rho_s = 1$.

A brief description of the flow is appropriate before proceeding to the comparisons. The bottom heating induces a thin hot boundary layer in which the density shows large variations due to the divergence of the thermal expansion coefficient of the SCF. This hot layer expands upward adiabatically compressing the rest of the fluid by thermoacoustic effects (the so called PE) leading to a fast increase of the temperature of the bulk fluid. Since the top plate temperature is kept at its initial value, a cold boundary layer settles along the top plate. As long as the flow is dominated by diffusion and by the PE, the thermal boundary layers grow in time at the heat diffusion speed; when the local Rayleigh number Ra, based on the hot boundary layer thickness h and on the temperature difference δT, exceeds a critical value Ra_c, a convective instability is triggered. This instability ends up in deforming the temperature and density fields with a number of thermal plumes rising from the thermal boundary layers and causing these latter to collapse; the flow becomes then convection dominated. The instability criterion of a SCF layer heated from below, established by Gitterman and Steinberg [5] and then discussed by Carlès and Ugurtas [6], is given by:

$$Ra = \frac{gh^4\beta\rho_c C_p}{\lambda\eta}\left[\frac{\delta T}{h} - \frac{gT_i\beta}{C_p}\right] \geqslant Ra_c \tag{6}$$

where β, λ, η, and C_p are respectively the thermal expansion coefficient, the thermal conductivity, the kinematic viscosity, and the heat capacity at constant pressure. The value of Ra_c depends on boundary conditions and is equal to 1100.6 for the present configuration. The term $gT_i\beta/C_p$ is the adiabatic temperature gradient obtained by moving a fluid particle along the hydrostatic pressure gradient [6]; it represents the stabilizing contribution of the Schwarzchild criterion commonly used in atmospheric sciences.

Both for the ALMN and CLMN approximations, Fig. 2 shows the evolutions of δT as a function of h for several heating cases. The thickness of the hot boundary layer is evaluated as the distance to the bottom plate where the local temperature reaches the bulk one with a relative difference less than 1%. The critical value of δT at which the convection arises is derived from the inequality (6) and plotted versus h (the thick solid line in Fig. 2) defining the zone of instability. A straight dashed line with a slop of (-3) represents the classical Rayleigh criterion also obtained through (6) but by removing the adiabatic temperature gradient term. In addition the symbol ending the evolution curve of $\delta T(h)$ corresponds to the instant when the hot boundary layer collapses. Nevertheless the convective instability arises much earlier; as the curve $\delta T(h)$ crosses into the instability zone, a number of convective cells appear near the bottom plate, the intensity of these vortices increases progressively until producing enough amount of convective transfer to deform the isotherms. We first notice that for a relatively strong heating ($\Delta T > 1$ mK) the flows predicted with both models are similar but not identical and the collapse of the thermal boundary layers occur at about the same time; this is due to the fact that a strong heating covers the

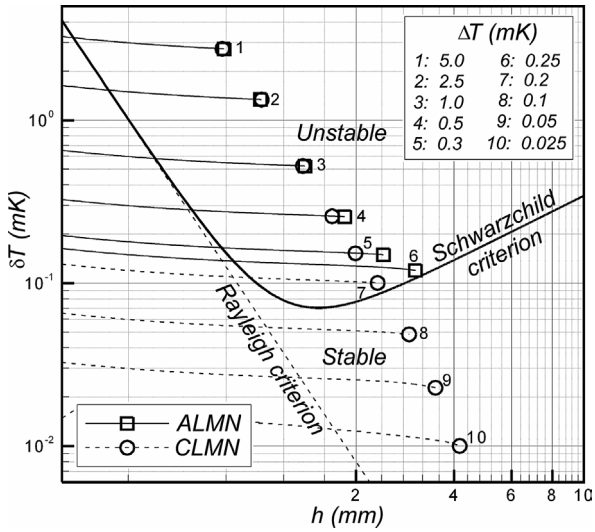

Fig. 2. Comparison between the ALMN model and the CLMN one for the prediction of the Rayleigh–Bénard convection thresholds in a SCF for several heating cases. The symbols correspond to the instants when the hot boundary layer collapses.

Fig. 2. Comparaison des modèles FNMA (≡ALMN) et FNMC (≡CLMN) pour la prédiction du déclenchement de la convection de Rayleigh–Bénard dans un FSC pour différents cas de chauffage. Les symboles correspondent aux instants d'effondrement de la couche limite chaude.

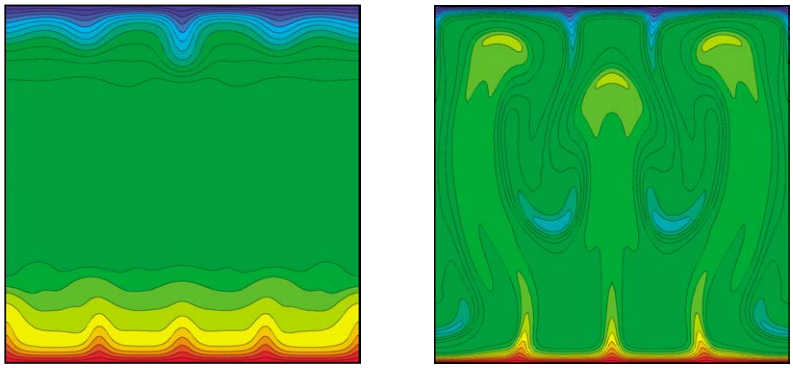

(a) (b)

Fig. 3. Comparison of the instantaneous temperature fields for $\Delta T = 0.3$ mK, $100t_{\mathrm{PE}}$ seconds after the collapse of the hot boundary layer. (a) ALMN, (b) CLMN.

Fig. 3. Comparaison des champs instantanés de température pour $\Delta T = 0{,}3$ mK, $100t_{\mathrm{EP}}$ secondes après l'effondrement de la couche limite chaude. (a) FNMA, (b) FNMC.

effects of stratification. The weight of this latter becomes more significant as the heating decreases; let us consider for example the case $\Delta T = 0.3$ mK. As far as synchronization is concerned, the collapse of the hot boundary layer is observed with about $90t_{\mathrm{EP}}$ seconds of time gap between the two models. Fig. 3 shows, for $\Delta T = 0.3$ mK, the instantaneous temperature fields $100t_{\mathrm{PE}}$ seconds after the collapse of the hot boundary layer for each model. Compared to those of Fig. 3(a) (ALMN), the thermal plumes are much more developed in 3(b) (CLMN) since their motion is not hindered by the stratification which, when taken into account, prevents the free growth of the plumes (3(a)). However for the considered heating intensity ($\Delta T = 0.3$ mK), the thermal plumes manage to deform the temperature field giving rise the slowly moving structures shown in Fig. 3(a). As the heating gets weaker

($\Delta T < 0.2$ mK here), the buoyant force being too weak to pull the fluid particles through the hydrostatic pressure gradient, the hot boundary layer predicted with the ALMN approximation remains stable. In return, not including the stratification, the CLMN model is unable to account for this stabilizing effect and persists in predicting a convective instability (according to the classical Rayleigh criterion) provided that the height L of the cavity allows enough growth of the thermal boundary layers.

6. Conclusion

This article described a low Mach number approximation for the modeling of a supercritical fluid buoyant flow induced by a weak heating. Including the density stratification, this model differs from the classical one in which the fluid compressibility is completely ignored. However, the assumption of small heating allows some simplifications and the resulting model requires no further numerical effort. In the Rayleigh–Bénard configuration, the proposed model takes account of the stabilizing effect of the hydrostatic pressure and predicts the convection threshold according to the criterion obtained by means of analytical analysis; it should allow the numerical investigation of the Schwarzchild instability.

Acknowledgements

The authors thank the financial support from CNES and the computational resources provided by IDRIS, the CNRS computing center.

References

[1] I. Raspo, B. Gilly, S. Amiroudine, P. Bontoux, B. Zappoli, Simulation of convective instabilities inside a supercritical fluid layer under Rayleigh–Bénard configuration, J. Chim. Phys. 96 (1999) 1059.
[2] S. Amiroudine, P. Bontoux, P. Larroudé, B. Gilly, B. Zappoli, Direct numerical simulation of instabilities in a two-dimensional near-critical fluid layer heated from below, J. Fluid Mech. 442 (2001) 119.
[3] G. Accary, I. Raspo, P. Bontoux, B. Zappoli, Three-dimensional Rayleigh–Bénard instability in a supercritical fluid, C. R. Mecanique 332 (2004) 209.
[4] A. Furukawa, A. Onuki, Convective heat transport in compressible fluids, Phys. Rev. E 66 (2002) 016302.
[5] M. Gitterman, V.-A. Steinberg, Criteria for the commencement of convection in a liquid close to the critical point, High Temp. (USSR) 8 (4) (1970) 754.
[6] P. Carlès, B. Ugurtas, The onset of free convection near the liquid–vapour critical point. Part I: Stationary initial state, Physica D 126 (1999) 69.
[7] A.-B. Kogan, H. Meyer, Heat transfer and convection onset in a compressible fluid: ^{3}He near the critical point, Phys. Rev. E 63 (2001) 056310.
[8] A.-B. Kogan, D. Murphy, H. Meyer, Onset of Rayleigh–Bénard convection in a very compressible fluid: ^{3}He, near Tc, Phys. Rev. Lett. 82 (1999) 4635.
[9] K. Nitsche, J. Straub, The critical hump of Cv under microgravity, results from D-Spacelab experiment 'Wärmekapazität', in: Proceedings of the 6th European Symp. on Material Sci. under Microgravity Conditions, ESA SP-256, 1987, p. 109.
[10] B. Zappoli, D. Bailly, Y. Garrabos, B. Le Neindre, P. Guenoun, D. Beysens, Anomalous heat transport by the piston effect in supercritical fluids under zero gravity, Phys. Rev. A 41 (1990) 2224.
[11] H. Boukari, J.-N. Schaumeyer, M.-E. Briggs, R.-W. Gammon, Critical speeding up in pure fluids, Phys. Rev. A 41 (1990) 2260.
[12] A. Onuki, H. Hao, R.-A. Ferrell, Fast adiabatic equilibration in a single-component fluid near the liquid–vapor critical point, Phys. Rev. A 41 (1990) 2256.
[13] B. Zappoli, The response of a nearly supercritical pure fluid to a thermal disturbance, Phys. Fluids A 4 (1992) 1040.
[14] S. Paolucci, On the filtering of sound from the Navier–Stokes equations, Technical report, Sandia National Laboratories USA, SAND82-8257, December 1982.
[15] G. Accary, I. Raspo, A 3D finite volume method for the prediction of a supercritical fluid buoyant flow in a differentially heated cavity, Computers & Fluids, in press.